energies

MDPI

Article

Resonant Combustion Start Considering Potential Energy of Free-Piston Engine Generator

Mitsuhide Sato *, Takumi Goto, Jianping Zheng and Shoma Irie

Faculty of Engineering, Shinshu University, Nagano-City, Nagano 380-8553, Japan;
18w2048c@shinshu-u.ac.jp (T.G.); 19w2081j@shinshu-u.ac.jp (J.Z.); 16t2020k@shinshu-u.ac.jp (S.I.)
* Correspondence: mitsuhide@shinshu-u.ac.jp; Tel.: +81-26-269-5211

Received: 30 August 2020; Accepted: 1 November 2020; Published: 3 November 2020



Abstract: Free-piston engine generators without a crank mechanism are expected to be used in series hybrid vehicles because of their lower losses. The series hybrid system requires a low starting thrust because the engine frequently starts depending on the battery state. This study clarifies the effectiveness of the constant thrust resonance starting method that utilizes the compression pressure of the engine and the spring thrust. The piston must pass the combustion starting point with a predetermined speed to start combustion. Herein, we present a thrust setting method that uses the energy state diagram to optimize the velocity at the combustion start point. A simulation is performed assuming output when mounted on a vehicle. Consequently, the simulation results show that the maximum thrust can be reduced by more than 90% compared to that without resonance. Moreover, the speed at the combustion start point is in agreement with the value obtained using an energy state diagram. An impulse-like combustion pressure is generated in 180 ms, and combustion can be started using resonance, as shown in an experiment using a small-output engine and linear motor. The effectiveness of the constant thrust resonance starting method was confirmed.

Keywords: free-piston engine; mechanical resonance; potential energy; mechanical energy; linear motor; combustion starting

1. Introduction

Transportation equipment emits large quantities of harmful gasses such as carbon dioxide and nitrogen oxide; therefore, the electrification of automobiles is progressing to improve the fuel efficiency of vehicles [1–5]. The development of pure electric vehicles, which are expected to be highly efficient, is progressing in countries around the world [6,7]. A series hybrid vehicle equipped with a dedicated engine for power generation and a rotary generator has been drawing attention in recent years because of a longer cruising range and lower costs [8–10]. In this system, the generator is driven by gasoline engine power, and the electric power obtained drives the vehicle propulsion motor to drive the vehicle. This is an electric vehicle that can extend the cruising range while generating electricity with a power generation engine. The energy density of fossil fuels, such as gasoline, is much higher than that of batteries. The number of batteries installed in the vehicle can be reduced by using a fossil fuel-based power generation system.

On the contrary, this system requires a linear motion conversion mechanism, such as a crank/camshaft, to convert the linear power of the engine into a rotational motion for the generator. The direct rotation conversion mechanism leads to mechanical loss and size increase. Therefore, studies on the free-piston engine linear generator system (FPEG) for improving the overall fuel efficiency are in progress [11–18]. The FPEG is an internal combustion engine that does not use a direct-drive rotation conversion mechanism. Using the combustion force of the engine and the repulsive force of the spring, the mover reciprocates to generate electricity with a linear generator.

The linear motion of the piston has been reported to be directly converted into energy without using the linear–rotation conversion mechanism, and the friction loss of the FPEG is improved by approximately 40% [11]. The efficiency of applying premixed compression ignition combustion was calculated using a combustion simulation, and an energy conversion efficiency of 42% was achieved under the conditions of 19.0 compression ratio and 12.7 kW power generation output [12]. The thrust is adjusted and the piston (i.e., the mover) without the crank can be operated arbitrarily by using the inverter current control of the linear generator [19]. Up to now, improvements in thermal and power generation efficiencies have been reported by taking advantage of arbitrary operability of piston [19–21].

The FPEG mainly required power generation; however, the linear generator is motored to drive the piston to start the engine from the time it is stopped until the engine is ignited [21]. Series hybrid vehicles do not keep the engine running all the time; instead, they turn on and off depending on the battery charge state. Therefore, a method for efficiently and steadily starting combustion is required considering many times of engine starting.

In other words, resonance using the repulsion spring and the spring effect with engine compression is appropriate for the combustion start process [22,23]. In ordinary spring resonance, the potential energy is bilaterally symmetrical at the center of vibration. In contrast, the potential energies of FPEGs in single-side engine type with different spring properties are not symmetrical, and the spring effect with the engine compression is nonlinear. Obtaining the amplification effect with a simple resonance is difficult because the resonance frequency during vibration is not constant. Thus, a constant thrust force is applied in the action direction to resonate the piston in opposed engine with symmetric potential energy [24]. An appropriate thrust must be given to start combustion at the combustion start point in single-side engine type; however, the method of setting the thrust has not yet been reported.

This study proposes a method of setting the constant thrust starting method using the energy state diagram concept. The thrust reduction effect of the constant thrust starting method is clarified by a simulation. We also perform experiments using an engine to verify whether or not the constant thrust resonance method can start an engine.

2. FPEG Operation Principle

2.1. Structure

Figure 1 presents the physical model of the FPEG consisting of a free-piston engine, a linear generator, and a repulsion spring. A major feature of the FPEG is the absence of a mechanical constraint, unlike the piston of the crank mechanism. The combustion force (F_c) of the engine acts on the piston, causing the free piston to move toward the spring repulsion chamber. The spring repulsion force (F_g) acts in the direction opposite to the combustion force and pushes the piston back into the combustion chamber. The piston reaches the combustion start point (x_s) near the top dead center (TDC) of the compression stroke and starts the combustion. The piston reciprocates between the TDC and the bottom dead center (BDC) to generate electricity by repeating this operation. The free piston engine burns properly by passing at the ideal piston speed at the combustion start point (x_s) [24].

The permanent magnet is attached to the piston, and the coil is wound on the stator, which constitutes a moving magnetic linear synchronous generator. The power is generated by the reciprocating motion of the piston, and the braking thrust (F_l) is applied to the piston. The dynamic braking thrust can be adjusted by power generation control using an inverter that controls the output to the battery. The linear generator thrust under vector control is expressed by the product of the q-axis current (i_q) and the thrust constant (K_f) of the generator. The equation of motion is described by Equation (1) with the piston displacement (x) and the piston mass (m).

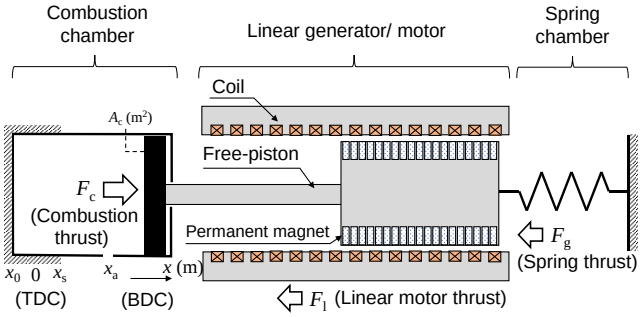


Figure 1. Physical model of the free-piston engine linear generator system (FPEG) consisting of a free-piston engine, a linear generator, and a repulsion spring. The position $x = 0$ means top dead center (TDC), $x = x_0$ means the leftmost end of the cylinder, $x = x_a$ means the scavenging point, and $x = x_s$ means the combustion start point in the compression stroke.

The spring repulsion force is expressed by Equation (2) with the spring repulsion coefficient (K_g). The combustion thrust is the product of the combustion chamber pressure and the cross-sectional area, as shown in Equation (3). The pressure after the combustion changes according to the thermodynamic law based on the heat generated and the volume of the combustion chamber. The pressure before the combustion behaves like an adiabatic compression air spring. The pressure on the starting process is expressed by Equation (4), with the pressure and volume at the scavenging point expressed as p_a (atmospheric pressure) and V_a, respectively.

Equation (4) describes the starting process before the start of the combustion and assumes that the compression behavior of the combustion chamber is a quasi-static air spring that does not exchange heat with the outer environment. Therefore, Equation (4) is based on Poisson's equation and describes the state at which the same gas is compressed. Equation (4) is transformed into Equation (5) with the scavenging point (x_a) and the length (x_0) from the TDC ($x = 0$) to the leftmost wall. The combustion thrust has a nonlinear relationship with the piston position [23].

$$m\frac{d^2x}{dt^2} = F_c - F_g + F_l \tag{1}$$

$$F_g = K_g x \tag{2}$$

$$F_c = A_c p_c \tag{3}$$

$$p_a V_a{}^\gamma = p_c V_c{}^\gamma \tag{4}$$

$$p_c = \frac{p_a V_a{}^\gamma}{V_c{}^\gamma} = \frac{p_a (x_a + x_0)^\gamma}{(x + x_0)^\gamma} \propto x^{-\gamma} \tag{5}$$

where m: piston mass (kg); x: piston position (m); F_c: combustion force (N); F_g: spring force (N); F_l: motor thrust (N); K_g: spring constant (N/m); A_c: combustion chamber cross-sectional area (m^2); p_c: combustion chamber pressure (Pa); V_c: combustion chamber volume (m^3); γ: heat capacity ratio (generally air standard condition 1.4); p_a: atmospheric pressure (Pa); V_a: scavenging point volume (m^3); and x_a: scavenging point position (m).

2.2. Starting

The piston must be operated from the stopped state to the combustion start point to burn the engine and start power generation in the FPEG. Therefore, the linear generator is driven as a linear motor on the engine start-up process (Figure 2). The piston is accelerated to a combustible speed using battery power.

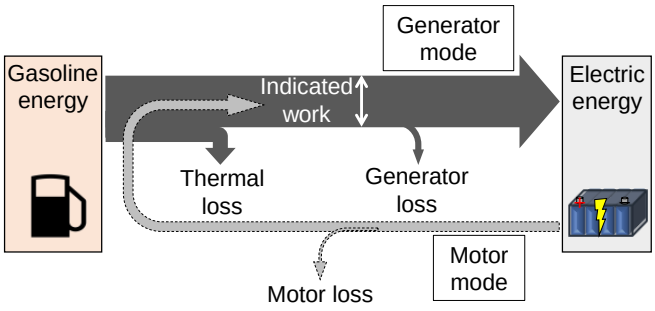


Figure 2. Energy flow of the FPEG. The linear generator is driven as a linear motor on the engine start-up process with battery power.

However, the piston speed must be increased up to the piston driving frequency (higher than 10 Hz by overcoming the repulsive spring thrust [11,12]. A large starting thrust is required to start the combustion in one stroke. A larger thrust increases the generator size and the power consumption. A hybrid vehicle particularly turns the engine on and off according to the remaining battery level. The starting thrust must be reduced because the number of engine starts in the hybrid vehicles is high.

2.3. Resonance Start-up

Mechanical resonance is effective for the starting thrust reduction. Figure 3 shows a comparison of the potential energies of a general spring–mass system and the FPEG. The left and right springs are given the same coefficient; therefore, the potential energy is line-symmetric with respect to the vibration center point in the spring–mass system model. On the contrary, the potential energy does not have line symmetry because the FPEG is composed of a linear mechanical spring and a non-linear compression spring effect in the combustion chamber. When a symmetrical linear spring force is applied, and the thrust of Equation (6) is applied at the resonance frequency of Equation (7), the equation of motion becomes Equation (8). The general solution of Equation (8) becomes Equation (9), and amplification occurs in the second-term component. However, the resonance frequency is not constant and changes depending on the vibration state because the potential energy of the FPEG is asymmetric. The resonance frequency of the spring changes in the FPEG with asymmetric potential energy, and the resonance is difficult to obtain with Equation (6).

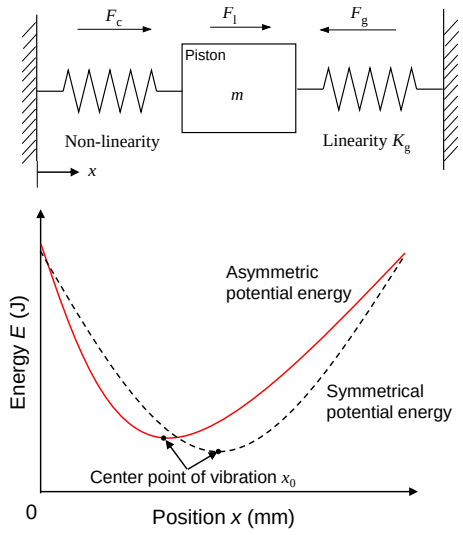


Figure 3. Comparison of the potential energies of a general spring–mass system and the FPEG. The potential energy does not have line symmetry in the FPEG.

Accordingly, a constant thrust is applied in the moving direction of the piston to amplify the pendulum amplitude, as shown in Figure 4, which presents the constant thrust resonance starting method. The thrust acts to the left in the expansion stroke from the TDC to the BDC, and to the right in the compression stroke from the BDC to the TDC. The thrust command gives a constant value by changing plus and minus according to the absolute piston speed value. A rightward thrust is applied on a positive piston speed, and whereas a leftward thrust is applied on a negative piston speed (Figure 1). This starting method realizes a resonance state. The piston then reaches the combustion start point with a small thrust.

$$F_l = F\cos\phi t \tag{6}$$

$$\omega = \phi = \sqrt{\frac{K_{g0}}{m}} \tag{7}$$

$$m\frac{d^2x}{dt^2} + \omega^2 x = F\cos\phi t \tag{8}$$

$$x(t) = C\cos(\omega t + \delta) + \frac{F}{2\omega}t\sin\omega t \tag{9}$$

where F: thrust amplitude (N); ω: resonance angular frequency (rad/s); ϕ: thrust angular frequency (rad/s); and K_{g0}: spring–mass system spring constant (N/m).

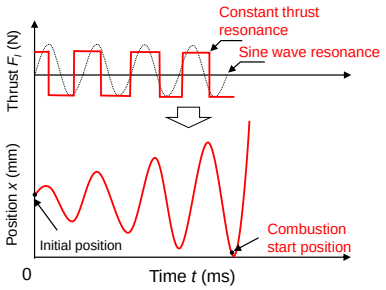


Figure 4. Constant thrust resonance starting method for the FPEG. A constant thrust is applied in the moving direction of the piston.

2.4. Consideration of Potential Energy

The thrust of the constant thrust resonance starting method must be set considering the characteristics of the spring and the speed of the combustion start point. However, a general solution for obtaining an appropriate thrust cannot be simply obtained because the combustion chamber pressure and spring force have nonlinear. Therefore, the state diagram of the potential energy given by the combustion chamber pressure and the spring force shown in Figure 5 is used.

Point a is the initial piston position. The piston advances to point b, where it balances with the potential energy while increasing the mechanical energy with a constant thrust by a linear motor to the piston in the direction of the BDC. After the piston changes its traveling direction, a constant thrust force acts in the direction of the TDC and the piston moves to point c. The piston then reaches the combustion start point z while increasing the mechanical energy by repeating this operation. The potential energy depends on the spring coefficient. The gradient of the mechanical energy of the piston depends on the starting thrust magnitude.

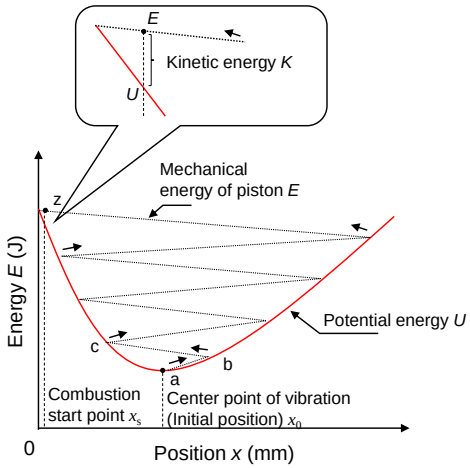


Figure 5. Energy diagram in the FPEG. The piston reaches the combustion start point z while increasing the mechanical energy by the given thrust of the linear motor.

The potential energies of the mechanical spring and the compression spring effect of the combustion chamber are given by Equations (10) and (11) by integrating Equations (2) and (4), respectively. The potential energy U in Figure 5 is the sum of Equations (10) and (11), as shown in Equation (12). The linear motor gives a constant thrust to the piston with the constant thrust resonance starting method. The piston gradually stores mechanical energy and can start combustion when the potential energy at the combustion start point is exceeded. The mechanical energy E of the piston is the sum of the potential U and kinetic K energies, as shown in Equation (13). The difference between the potential energy at the combustion start point and the mechanical energy is the kinetic energy. The starting thrust must be set to obtain the speed required for a proper start of combustion. The starting thrust can be set such that the velocity at the combustion start point v_s is ideal with the energy state diagram and the kinetic energy of Equation (14).

$$U_g = \frac{1}{2} K_g x^2 \tag{10}$$

$$\begin{aligned} U_c = \int_x^{x_a} F_c dx = \left[p_a A_c (x_a + x_0)^\gamma \frac{1}{-\gamma+1} (x + x_0)^{-\gamma+1} \right]_x^{x_a} \ (\gamma \neq 1) \\ U_c = \int_x^{x_a} F_c dx = \left[p_a A_c (x_a + x_0) ln(x + x_0) \right]_x^{x_a} \ (\gamma = 1) \end{aligned} \tag{11}$$

$$U = U_g + U_c \tag{12}$$

$$E = U + K \tag{13}$$

$$v_s = \sqrt{\frac{2K}{m}} \tag{14}$$

where U_g: potential energy of the mechanical spring (J); U_c: potential energy of compression in the combustion chamber (J); x_0: distance between the TDC and the leftmost point (m), U: total potential energy (J); E: mechanical energy (J); K: kinetic energy (J); and v_s: velocity at the combustion starting position (m).

3. Starting Thrust Reduction Effect

This chapter clarifies the thrust reduction effect of the constant thrust resonance starting method using a simulation. We also show herein that the velocity at the combustion start point reaches a desired value by setting the thrust using the energy state diagram. The simulation was conducted at an output of 10 kW, simulating the conditions of installing this system in a car.

3.1. Simulation Conditions

The simulation is performed by assuming a 10 kW output considering vehicle installation [11,12]. Figure 6 shows a block diagram of the motion analysis constructed using MATLAB-Simulink. The simulation combines the electric circuit of the motor, vector control and, equation of motion, as shown Equation (1) [19]. The linear generator (linear motor) uses vector control. The starting thrust can be controlled by changing the q-axis current. Table 1 presents the mechanical conditions of the simulation. As the frictional force before combustion is small and does not show significant fluctuations [11], the friction was not considered in the simulation. Mechanical springs have low damping [25]. Damping action is expected when the combustion chamber is used as an air spring before the start of combustion. However, in the experiment described in Section 4, the pressure damping of the air spring before the start of combustion was small. Therefore, the damping of the spring was not considered in the simulation. The starting point is set to the position at which the potential energy is minimum.

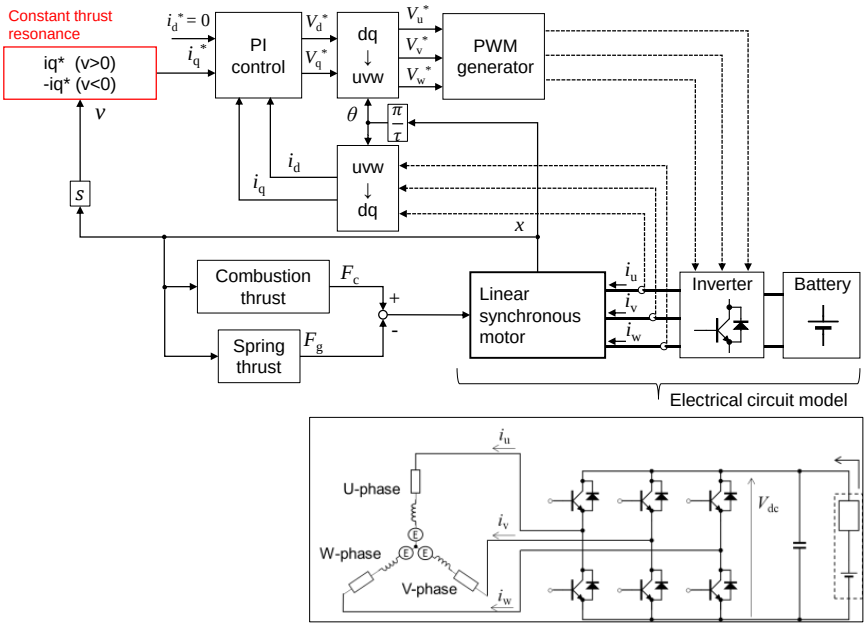


Figure 6. Block diagram of the FPEG simulation.

Table 1. Mechanical conditions of the simulation.

Item	Value
Piston and mover mass m	5.25 kg
Distance between TDC and the leftmost point x_0	7 mm
Bore cross section A_c	0.00363 m^2
Exhaust point position x_a	70 mm

Figure 7 depicts the basic configuration of the linear generator [20]. Table 2 shows the linear generator specifications obtained with the electromagnetic field analysis software JMAG-Designer. The linear generator is designed considering the copper loss reduction and miniaturization for the vehicle mounting [26–30] and is a magnet-movable cylindrical linear synchronous generator. A rectangular wire is used as the coil wire to increase the space factor. It has a concentrated winding structure put in one tooth to reduce the copper loss [31–33]. The magnetic flux of the magnet is concentrated on the stator side with a Halbach array to improve the thrust constant [34–36].

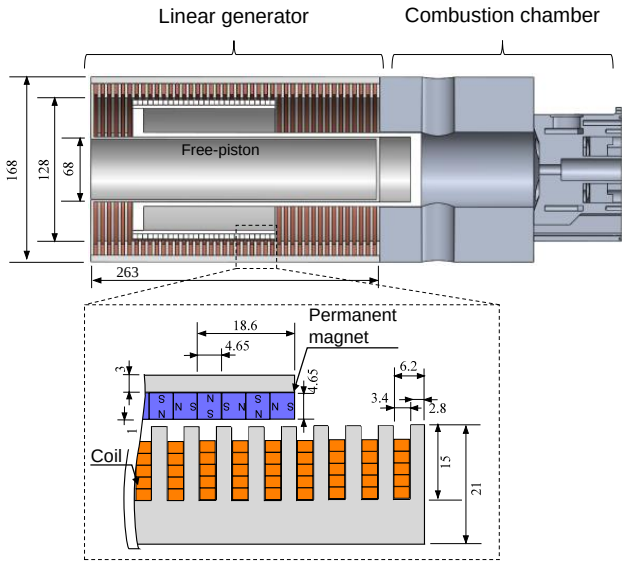


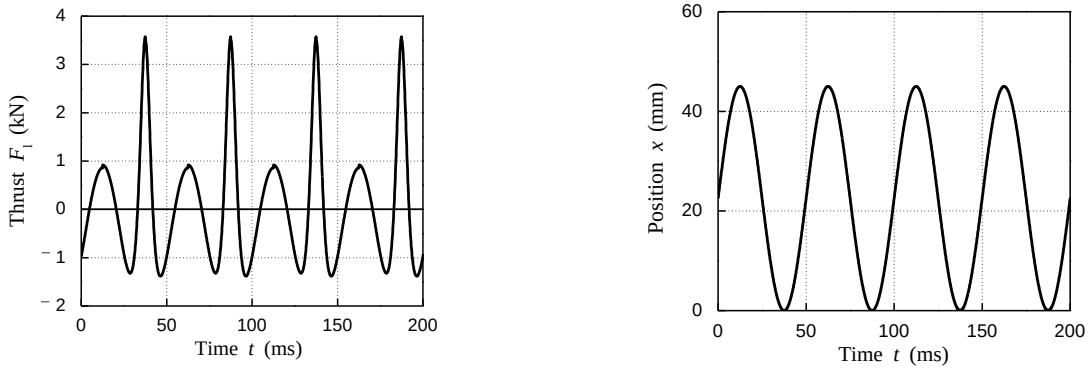
Figure 7. Basic configuration of the linear generator for the 1 kW output.

Table 2. Linear generator specifications.

Item	Value
Stator external dimensions	168 × 263 mm
Outer dimensions of mover	128 × 130 mm
Armature resistance	108 mΩ (per phase)
Armature inductance	1.8 mH (per phase)
Thrust constant	22 N/A

3.2. Simulation Results

Figure 8 shows the thrust that started the engine with one stroke, in which the engine was immediately driven at 20 Hz from the piston stopped state to the combustion start point. A very large thrust of 3.5 kN is required at 80 mm stroke and 20 Hz drive frequency.



(**a**) (**b**)

Figure 8. Simulation results with the starting engine in one stroke: (**a**) linear motor thrust and (**b**) piston position. A large thrust of more than 3 kN is required to reach the combustion start point in one stroke.

The sinusoidal thrust of Equations (6) and (7) is applied by the linear motor to reduce the starting thrust. Figure 9 shows the simulation results. A sinusoidal thrust with 150 N amplitude and 20 Hz frequency is applied as shown in Figure 8. In the figure, panel (b) illustrates the displacement.

The displacement can gradually increase up to 250 ms, but the amplitude attenuates after 250 ms because the compression spring effect in the combustion chamber is nonlinear, and the spring resonance frequency is not constant. The spring effect the combustion chamber compression has no linearity, and the potential energy is not line-symmetric; therefore, the resonance using the sinusoidal thrust is difficult in the FPEG. Consequently, reaching the combustion starting point in a stable manner in the sinusoidal thrust starting method is difficult.

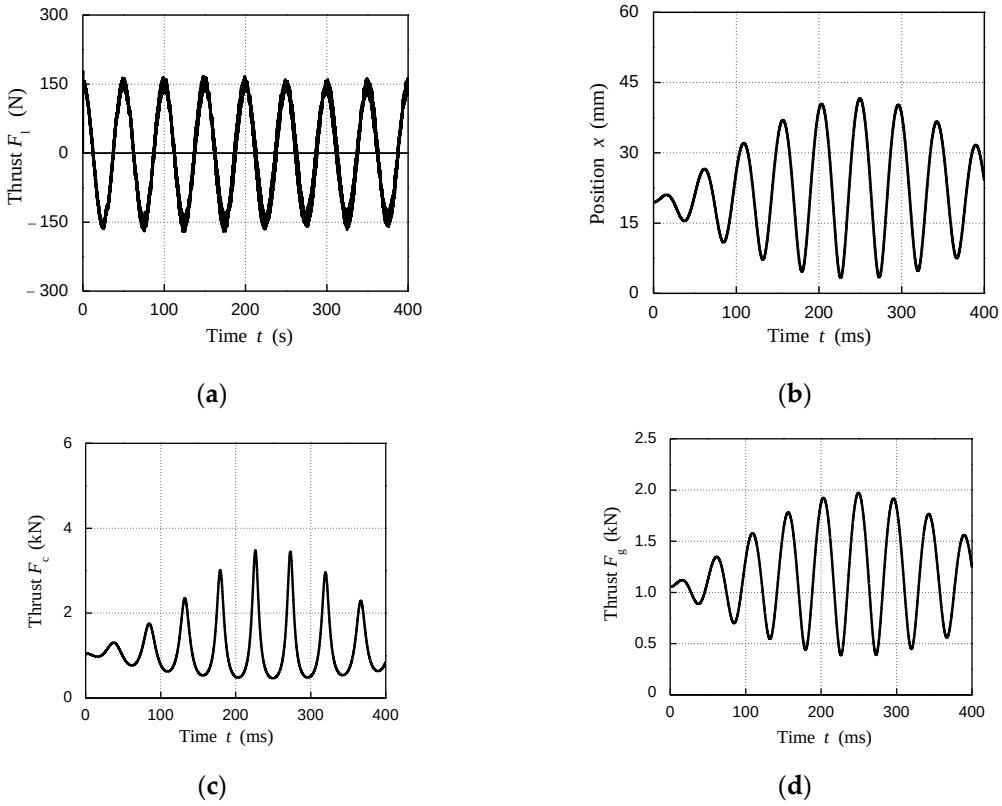


Figure 9. Simulation results with sinusoidal thrust: (**a**) linear motor thrust; (**b**) piston position; (**c**) combustion chamber thrust; (**d**) spring thrust. The piston position can gradually increase up to 250 ms, but the amplitude attenuates after 250 ms.

The propriety of amplification and the thrust reduction effect of the constant thrust resonance starting method described in Section 2 have been confirmed. Table 3 presents the simulation conditions. Nos. 2 and 3 change the starting thrust with the same spring constant as no. 1, while the spring constant of the mechanical spring and starting thrust change nos. 4 and 5. The starting thrust is set using the energy state diagram in Figure 10 and the energy law in Equation (13), such that the number of vibrations and the starting speed would be the expected values. Cases 1, 2, and 3 have the same spring characteristics, but different starting thrusts; therefore, the potential energies are the same, and the mechanical energy gradient is different. In Cases 4 and 5, the potential energy differs by changing the spring characteristics, but the number of starts is the same as in Case 1. In addition, the starting point speed v_s was 1.2 m/s under these conditions. This speed reflects the readiness to combust at minimum starting displacement, which depends on the conditions.

Table 3. Conditions for the simulation and expected results.

Case	Spring Constant	Starting Thrust	Expected Number of Vibrations to Start	Expected Velocity at the Combustion Start Point
1	41,453 N/m	125 N	4	
2	41,453 N/m	168 N	3	
3	41,453 N/m	256 N	2	−1.2 m/s
4	30,000 N/m	167 N	3	
5	50,000 N/m	175 N	3	

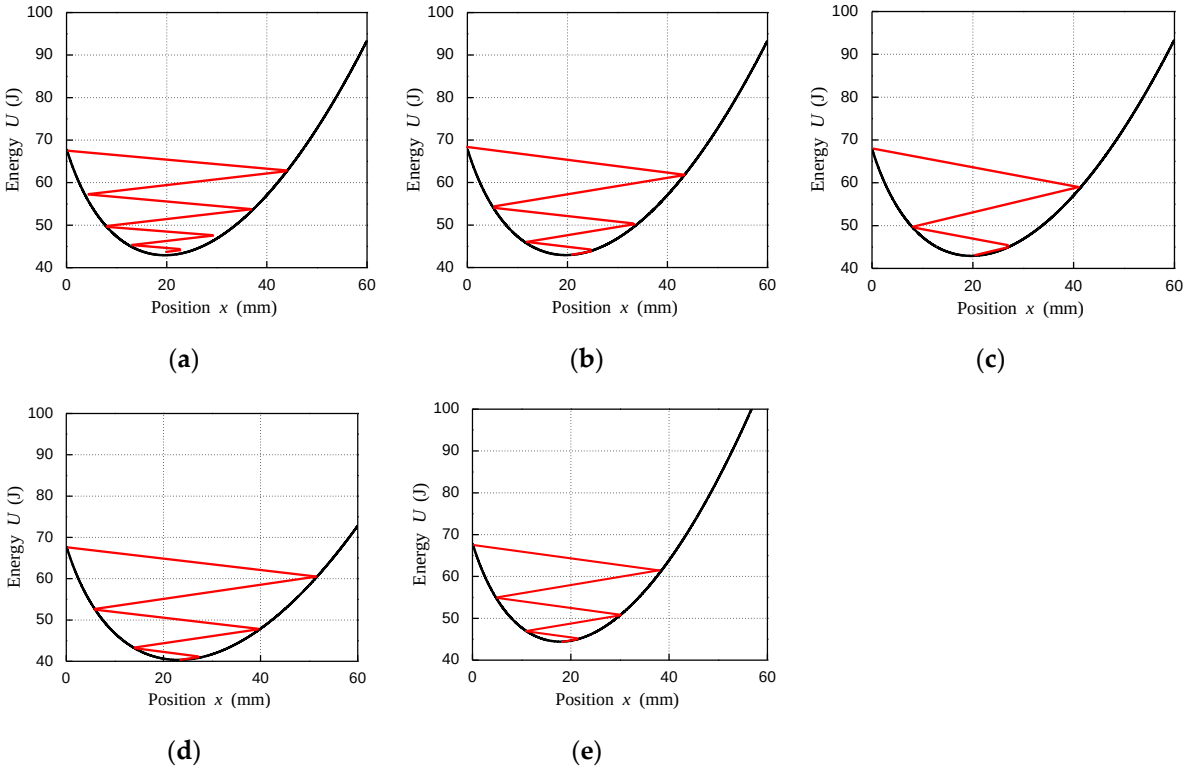
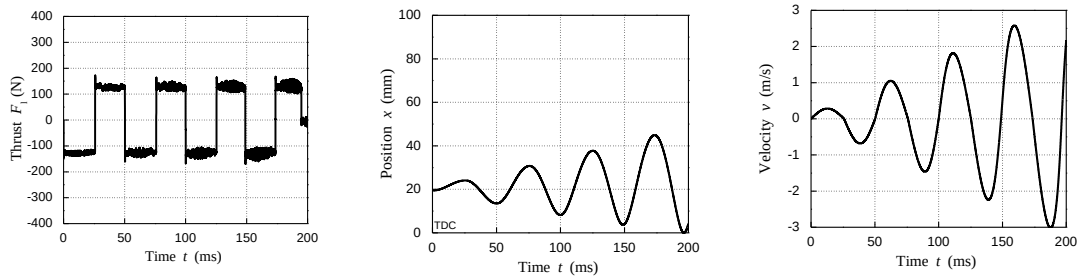
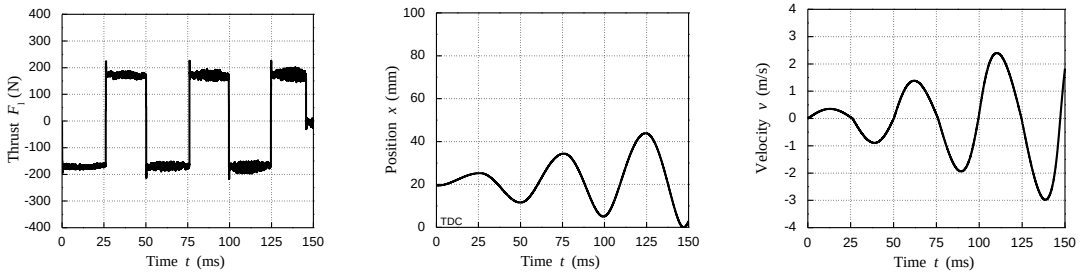


Figure 10. Energy state diagram: (**a**) Case 1, (**b**) Case 2, (**c**) Case 3, (**d**) Case 4, and (**e**) Case 5. The black curve is potential energy. The red line is the mechanical energy of the piston.

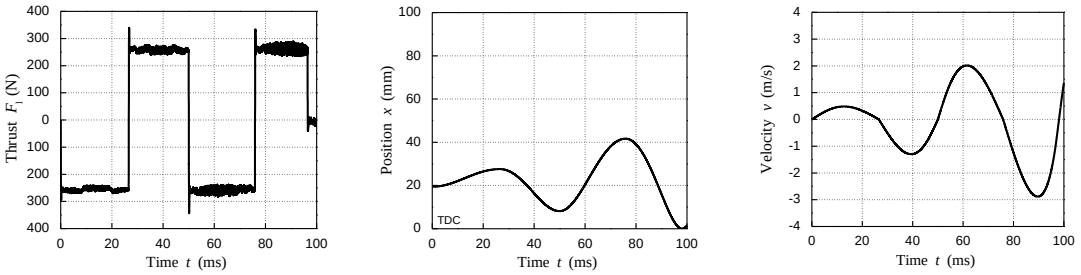
Figure 11 shows the simulation results of the constant thrust resonance starting method. The first to fifth lines depict Cases 1–5, respectively. Column (a) shows the starting thrust of the linear motor, which acts uniformly in the direction of the piston action in all conditions. Figure 11b,c shows the piston displacement and speed. The amplitude gradually increases because of resonance, and the piston can reach the combustion start point with a thrust much smaller than that in Figure 8. Using resonance is practically considered to have no issues because the piston can reach the combustion start point within 0.2 s in all cases. The number of vibrations required before starting is also the same as the number of times assumed in Table 3. Increasing the thrust is effective in shortening the starting time and reducing the number of start-up vibrations.



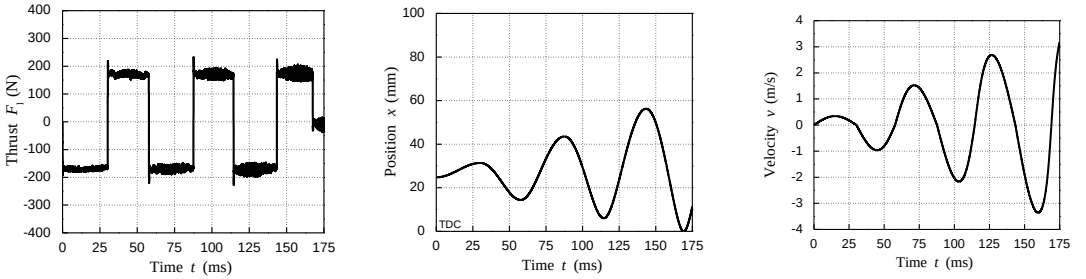
(**a**)



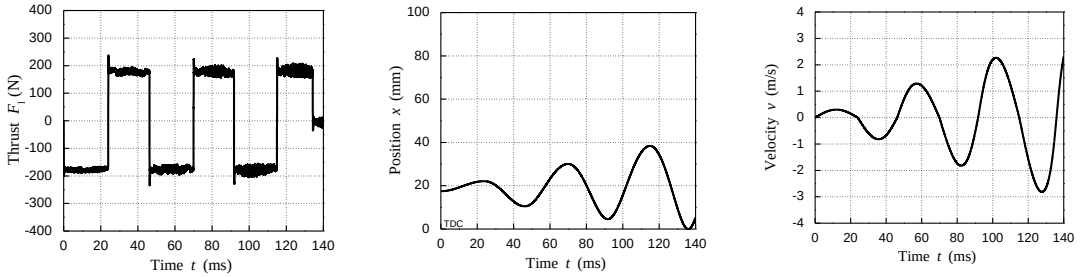
(**b**)



(**c**)



(**d**)



(**e**)

Figure 11. Simulation results of the thrust of the linear motor, piston position, and piston velocity with the constant thrust resonance starting method: (**a**) Case 1, (**b**) Case 2, (**c**) Case 3, (**d**) Case 4, and (**e**) Case 5. The amplitude gradually increased because of resonance. The piston can reach the combustion start point with much a smaller thrust.

Figure 12 illustrates a diagram of the piston position and velocity with an enlarged view of the vicinity of the combustion start point. The amplitude increases while passing points a, b, and c from the starting point, and the piston reaches the combustion starting point z. The piston velocity at the combustion start point reaches 1.2 m/s, which is the expected result. The phase diagram appears distorted because the potential energies in cases 4 and 5 were different from those in cases 1–3.

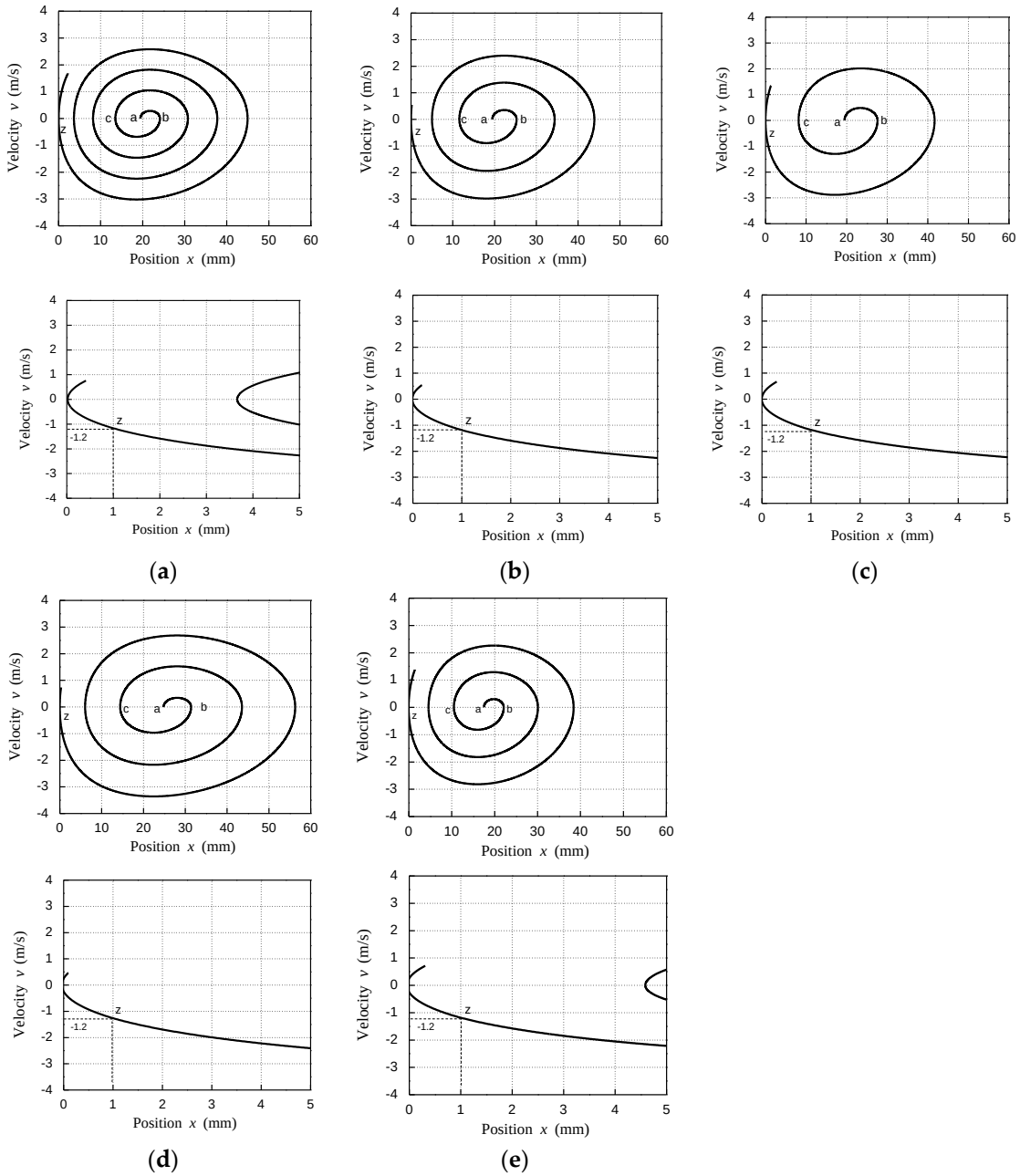


Figure 12. Simulation results of a diagram of the piston position and velocity. The bottom of each figure shows an enlarged view of the vicinity of the combustion start point: (**a**) Case 1, (**b**) Case 2, (**c**) Case 3, (**d**) Case 4, and (**e**) Case 5. The piston velocity at the combustion start point was 1.2 m/s, as predicted in the energy state diagram.

The constant thrust starting method using resonance reduces the maximum thrust required to start the engine from 3.5 kN to several hundred N. It is also practically effective for changing the thrust value considering the combustion start time. In addition, the number of reciprocations up to the start

and the velocity at the combustion start point predicted using the energy state diagram agree with the simulation results. Therefore, the thrust can be set considering the conditions required for starting using the energy state diagram.

4. Engine Start Experiment

This chapter shows that the constant thrust resonance start method can start combustion by using an experimental device with a small engine and a linear motor.

4.1. Experimental Method

Figure 13a shows the moving part of the engine experimental device comprising a linear motor that gives a starting thrust, an engine, and a mechanical spring. The engine piston and the mover of the linear motor are mechanically connected. A mechanical spring is attached to the other side of the engine. The spring constant K_g and spring preload were 9940 N/m and 150 N, respectively.

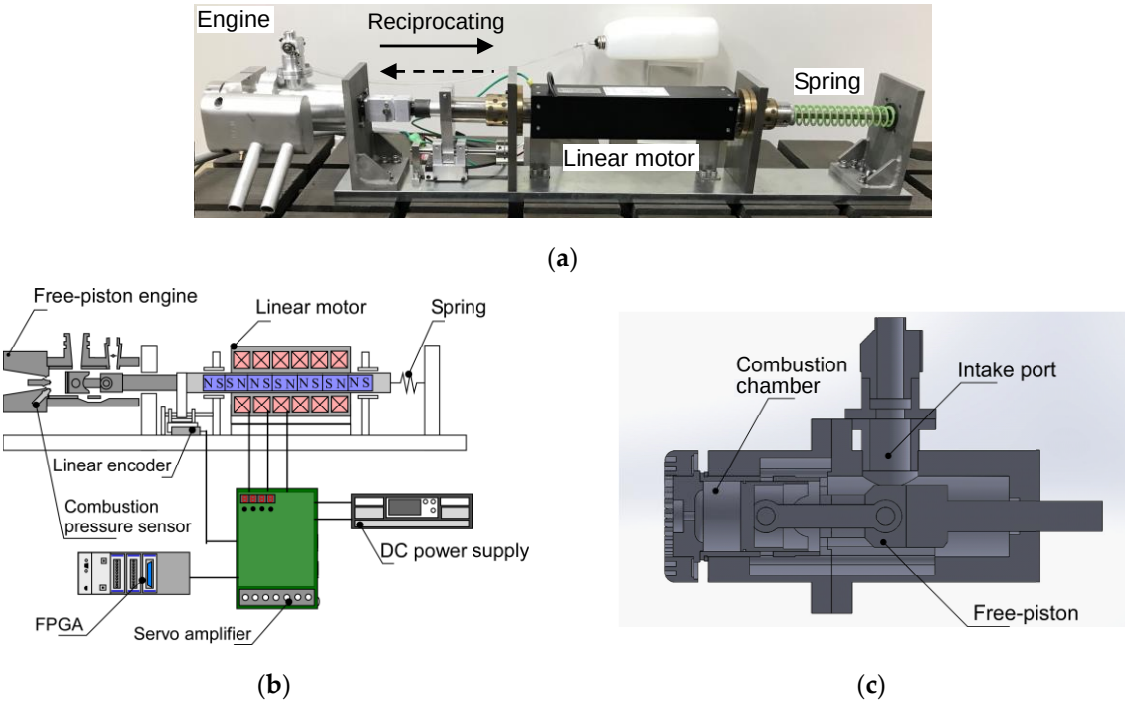


Figure 13. Experimental device: (**a**) appearance of moving parts, (**b**) overall structure, and (**c**) cross section of the engine interior. This device consists of a linear motor that gives a starting thrust, an engine, and a mechanical spring. The output of the engine is about 1.7 kW, and the linear motor controls the thrust with an FPGA and an amplifier.

Figure 13b shows the overall structure of the engine test equipment. A shaft motor (S350-1S-100st-L480, GMC Hillstone co., Ltd., Yamagata, Japan) is used as the linear motor giving the starting thrust. An FPGA real-time controller and a servo amplifier are used for the linear motor thrust control. The servo amplifier controls the current flowing through the linear motor by the PWM control based on the thrust command created by the FPGA. A combustion pressure sensor (CAS-15K, CITIZEN FINEDEVICE Co., Ltd., Yamanashi, Japan) is attached to the engine to measure the pressure inside the combustion chamber. A magnetic linear encoder (LA11D, Renishaw plc) is used to measure the piston position.

Figure 13c displays the engine interior cross-section. Table 4 shows the engine specifications. A glow-ignition, two-cycle engine (180X TN, Enya Metal Products Co., Ltd., Saitama, Japan) was used to confirm reaching the TDC and starting the combustion by using resonance without adjusting the

ignition time. The fuel used KLOTZ for a small glow engine, which is mainly composed of methanol, nitromethane and oil. The fuel contains 15% nitromethane and 22% oil. The target velocity at the start of combustion is set at 0.5 m/s, which is obtained from the engine operation test results.

Table 4. Engine specifications.

Item	Value
Displacement	36 cm^3
Bore diameter	34 mm
Exhaust point position	25 mm
Piston stroke	40 mm
Maximum output	1.73 kW

4.2. Experimental Results

Figure 14 illustrates the experimental results. Panel (a) depicts the thrust applied to the piston, panel (b) shows the piston displacement, panel (c) exhibits the combustion chamber pressure, panel (d) shows combustion pressure vs. piston position in the starting process in about 100 ms, and panel (e) exhibits the piston position calculated by simulation. A thrust of 280 N was applied in the same direction of the mover movement while using the start method that employs resonance. The piston movement amplitude gradually increases because of the spring resonance. The compression and expansion pressures at the engine starting stroke have approximately the same curve with damping energy less than 1J and a small effect of damping effect. The combustion chamber pressure operates like an air spring before the start of combustion. The inside of the cylinder was compressed with approaching TDC and a state close to combustion occurred at approximately 150 ms. An impulsive combustion pressure is generated at 180 ms due to the piston reaching TDC, and the engine combustion is confirmed to have been started using the spring resonance. The maximum combustion pressure at this time was 5.6 MPa. The number of reciprocations up to the start of the combustion is four, and the combustion start speed was 1.22 m/s, which is in close agreement with the set conditions. The speed error is approximately 1.7%, which is within acceptable range. The cause of the error in the combustion start speed is the effect of friction and damping effect of air spring.

Figure 14d shows the relationship pressure of the combustion chamber and the piston stroke on the starting process around 100 ms. Similar curves were obtained during compression and expansion, and the effect of attenuation is small. Moreover, the specific heat ratio of both pressure-curves were calculated using an approximate curve, they were 1.21 and 1.23 at the time of expansion and compression, respectively. Contrary to the simulation, the specific heat ratio during the actual operation slightly differs between compression and expansion. This is one of the causes of the error of 1.7% of the combustion start speed. Thus, the accuracy of combustion start velocity can be increased by obtaining the specific heat ratio in advance using the pressure history. The simulation was conducted under the conditions simulating the experimental environment. The simulation results confirmed that the piston movement was amplified by the constant thrust starting method and reached the TDC after four reciprocating movements as in the experiment. The amplitude of the simulation was slightly larger than that of the experiment because the damping effect and friction of the combustion chamber were not taken into consideration.

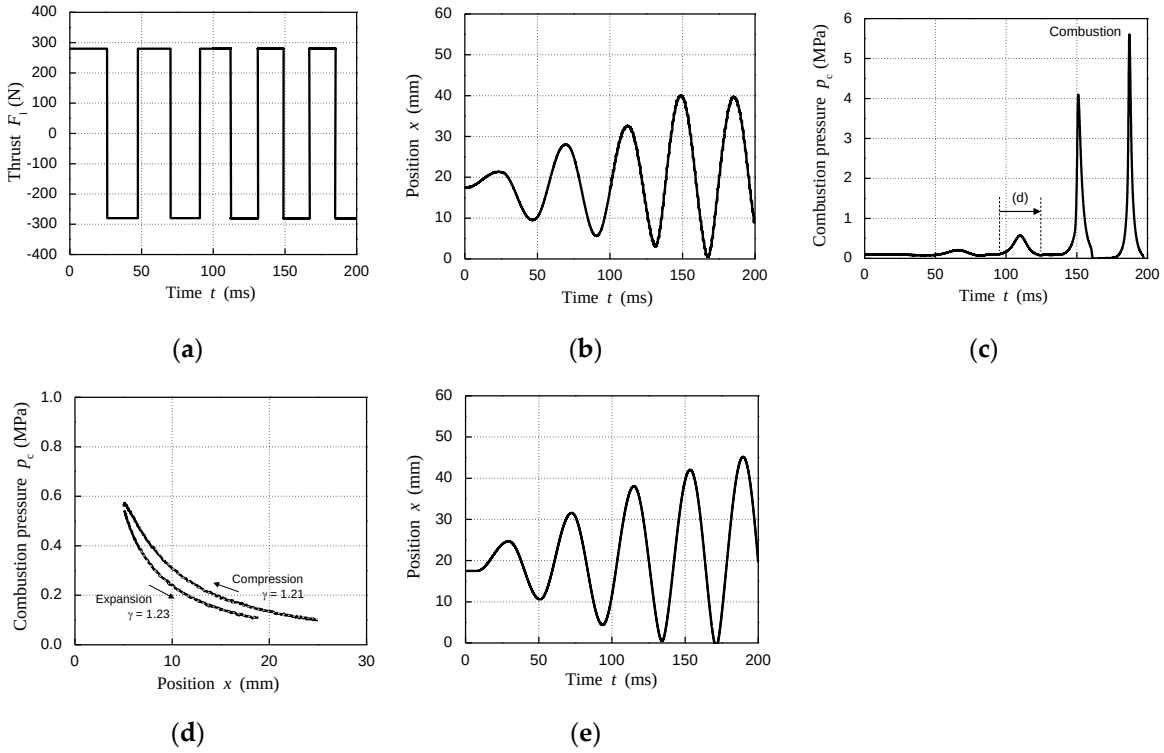


Figure 14. Experimental results with the constant thrust resonance starting method: (**a**) linear motor thrust, (**b**) piston position, (**c**) combustion pressure, (**d**) combustion pressure vs. piston position in the starting process, and (**e**) piston position calculated by simulation. An impulse-like combustion pressure could be generated in approximately 180 ms with the constant thrust starting method.

5. Conclusions

To start power generation with the FPEG, the piston must be given thrust up to the stroke and speed at which combustion can start. A very large thrust is required to make the stopped piston ready for combustion. Therefore, we used herein spring resonance to gradually increase the amplitude.

The piston resonates by utilizing the compression spring effect of the combustion chamber and the spring effect of the spring chamber. However, the potential energy of the FPEG is not symmetrical about the center of vibration and using a simple spring–mass resonance system is difficult. Therefore, we used the constant thrust resonance starting method, in which thrust is applied in the same direction as the piston action direction.

The constant thrust resonance starting method had a maximum thrust reduction effect of more than 90% compared to the starting method by one stroke without using resonance and enables a stable amplification. The number of reciprocations and the combustion start speed predicted using the energy state diagram were in agreement with the simulation results. The starting thrust can be set appropriately by using the energy state diagram. This method is also effective for the opposed engine model in which the potential energy is symmetrical.

We confirmed that the constant thrust starting method can start the engine combustion with a small-output experimental device using a free-piston engine. The amplitude of the piston displacement gradually increased from the position of the natural length of the spring, and the combustion started at the combustion start point when a constant was applied thrust in the direction of the piston action. The combustion can be started by reducing the starting-up thrust through a proper utilization of the constant thrust resonance starting method.

Author Contributions: Conceptualization and methodology, M.S.; software, M.S., T.G., and J.Z.; validation, T.G., J.Z., and S.I.; writing—original draft preparation, M.S. and T.G.; funding acquisition, M.S. All authors have read and agreed to the published version of the manuscript.

Funding: This work was supported by JSPS KAKENHI Grant Number 20K14714. This work was partially supported by Nagamori Foundation research grant 2020.

Conflicts of Interest: The authors declare no conflict of interest.

References

1. Coloma, J.F.; García, M.; Wang, Y.; Monzón, A. Environmental Strategies for Selecting Eco-Routing in a Small City. *Atmosphere* **2019**, *10*, 448. [CrossRef]
2. Serrano, J.R. Imagining the Future of the Internal Combustion Engine for Ground Transport in the Current Context. *Appl. Sci.* **2017**, *7*, 1001. [CrossRef]
3. El-Taweel, N.A.; Khani, H.; Farag, H.E.Z. Analytical Size Estimation Methodologies for Electrified Transportation Fueling Infrastructures Using Public–Domain Market Data. *IEEE Trans. Transp. Electr.* **2019**, *5*, 840–851. [CrossRef]
4. Monteiro, V.; Afonso, J.A.; Ferreira, J.C.; Afonso, J.L. Vehicle Electrification: New Challenges and Opportunities for Smart Grids. *Energies* **2019**, *12*, 118. [CrossRef]
5. Kang, H.; Kim, S.; Lee, K. Multiple Harmonics Reduction Method for the Integrated On-board Battery Charging System of Hybrid Electric Vehicles. *IEEJ J. Ind. Appl.* **2020**, *9*, 235–243. [CrossRef]
6. Varga, B.O.; Sagoian, A.; Mariasiu, F. Prediction of Electric Vehicle Range: A Comprehensive Review of Current Issues and Challenges. *Energies* **2019**, *12*, 946. [CrossRef]
7. Zhu, J.; Wierzbicki, T.; Li, W. A review of safety-focused mechanical modeling of commercial lithium-ion batteries. *J. Power Sources* **2018**, *378*, 153–168. [CrossRef]
8. Yu, Y.; Jiang, J.; Min, Z.; Wang, P.; Shen, W. Research on Energy Management Strategies of Extended-Range Electric Vehicles Based on Driving Characteristics. *World Electr. Veh. J.* **2020**, *11*, 54. [CrossRef]
9. Kim, D.; Benoliel, P.; Kim, D.; Lee, T.H.; Park, J.W.; Hong, J. Framework Development of Series Hybrid Powertrain Design for Heavy-Duty Vehicle Considering Driving Conditions. *IEEE Trans. Veh. Technol.* **2019**, *68*, 6468–6480. [CrossRef]
10. Passalacqua, M.; Carpita, M.; Gavin, S.; Marchesoni, M.; Repetto, M.; Vaccaro, L.; Wasterlain, S. Supercapacitor Storage Sizing Analysis for a Series Hybrid Vehicle. *Energies* **2019**, *12*, 1759. [CrossRef]
11. Jia, B.; Mikalsen, R.; Smallbone, A.; Roskilly, A.P. A study and comparison of frictional losses in free-piston engine and crankshaft engines. *Appl. Ther. Eng.* **2018**, *140*, 217–224. [CrossRef]
12. Kosaka, H.; Akita, T.; Moriya, K.; Goto, S.; Hotta, Y.; Umeno, T.; Nakakita, K. *Development of Free Piston Engine Linear Generator System Part 1—Investigation of Fundamental Characteristics*; SAE Technical Papers 2014-01-1203; SAE International: Warrendale, PA, USA, 2014.
13. Moriya, K.; Goto, S.; Akita, T.; Kosaka, H.; Hotta, Y.; Nakakita, K. *Development of Free Piston Engine Linear Generator System Part 3—Novel Control Method of Linear Generator for to Improve Efficiency and Stability*; SAE Technical Papers 2016-01-0685; SAE International: Warrendale, PA, USA, 2016.
14. Xu, Z.; Chang, S. Prototype testing and analysis of a novel internal combustion linear generator integrated power system. *Appl. Energy* **2010**, *87*, 1342–1348. [CrossRef]
15. Goto, S.; Moriya, K.; Kosaka, H.; Akita, T.; Hotta, Y.; Umeno, T.; Nakakita, K. *Development of Free Piston Engine Linear Generator System Part 2—Investigation of Control System for Generator*; SAE Technical Papers 2014-01-1193; SAE International: Warrendale, PA, USA, 2014.
16. Hung, N.B.; Lim, O.; Iida, N. The effects of key parameters on the transition from si combustion to hcci combustion in a two-stroke free piston linear engine. *Appl. Energy* **2015**, *137*, 385–401. [CrossRef]
17. Li, Q.; Xiao, J.; Huang, Z. Simulation of a Two-Stroke Free-Piston Engine for Electrical Power. *Energy Fuels* **2008**, *22*, 3443–3449. [CrossRef]
18. Yuan, C.; Feng, H.; He, Y.; Xu, J. Combustion characteristics analysis of a free-piston engine generator coupling with dynamics and scavenging. *Energy* **2016**, *102*, 637–649. [CrossRef]
19. Sato, M.; Nirei, M.; Yamanaka, Y.; Murata, H.; Bu, Y.; Mizuno, T. Operation Range of Generation Braking Force to Achieve High Efficiency Considering Combustion in a Free-Piston Engine Linear Generator System. *IEEJ J. Ind. Appl.* **2018**, *7*, 343–350. [CrossRef]

20. Yamanaka, Y.; Nirei, M.; Sato, M.; Murata, H.; Bu, Y.; Mizuno, T. Design of a Linear Synchronous Generator and Examination of the Driving Range for a Free-Piston Engine Linear Generator System. *IEEJ J. Ind. Appl.* **2018**, *7*, 351–357. [CrossRef]
21. Sato, M.; Naganuma, K.; Nirei, M.; Yamanaka, Y.; Suzuki, T.; Goto, T.; Bu, Y.; Mizuno, T. Improving the Constant-Volume Degree of Combustion Considering Generatable Range at Low-speed in a Free-Piston Engine Linear Generator System. *IEEJ Trans. Electr. Electron. Eng.* **2019**, *14*, 1703–1710. [CrossRef]
22. Wang, X.; Chen, F.; Zhu, R.; Yang, G.; Zhang, C. A Review of the Design and Control of Free-Piston Linear Generator. *Energies* **2018**, *11*, 2179. [CrossRef]
23. Jia, B.; Zuo, Z.; Feng, H.; Tian, G.; Roskilly, A.P. Investigation of the starting process of free-piston engine generator by mechanical resonance. *Energy Procedia* **2014**, *61*, 572–577. [CrossRef]
24. Jia, B.; Zuo, A.; Feng, H.; Tian, G.; Smallbone, A.; Roskilly, A.P. Effect of closed-loop controlled resonance based mechanism to start free piston engine generator: Simulation and test results. *Appl. Energy* **2016**, *164*, 532–539. [CrossRef]
25. Yan, H.; Wang, D.; Xu, Z. *Design and Simulation of Opposed-Piston Four-Stroke Free-Piston Linear Generator*; SAE Technical Papers 2015-01-1277; SAE International: Warrendale, PA, USA, 2015.
26. Sun, P.; Zhang, C.; Chen, J.; Zhao, F.; Liao, Y.; Yang, G.; Chen, C. Decoupling design and verification of a free-piston linear generator. *Energies* **2016**, *9*, 1067. [CrossRef]
27. Wang, J.; West, M.; Howe, D.; Parra, Z.D.L.; Arshad, W.M. Design and experimental verification of a linear permanent magnet generator for a free-piston energy converter. *IEEE Trans. Energy Convers.* **2007**, *22*, 299–306. [CrossRef]
28. Zheng, P.; Tong, C.; Bai, J.; Yu, B.; Sui, Y.; Shi, W. Electromagnetic design and control strategy of an axially magnetized permanent-magnet linear alternator for free-piston stirling engines. *IEEE Trans. Ind. Appl.* **2013**, *48*, 2230–2239. [CrossRef]
29. Cao, R.; Cheng, M.; Mi, C.C.; Hua, W. Influence of leading design parameters on the force performance of a complementary and modular linear flux-switching permanent-magnet motor. *IEEE Trans. Ind. Electr.* **2014**, *61*, 2165–2175. [CrossRef]
30. Zheng, P.; Tong, C.; Chen, G.; Liu, R.; Sui, Y.; Shi, W.; Cheng, S. Research on the magnetic characteristic of a novel transverse-flux pm linear machine used for free-piston energy converter. *IEEE Trans. Magn.* **2011**, *47*, 1082–1085. [CrossRef]
31. Wang, Q.; Zhao, B.; Zou, J.; Li, Y. Minimization of Cogging Force in Fractional-Slot Permanent Magnet Linear Motors with Double-Layer Concentrated Windings. *Energies* **2016**, *9*, 918. [CrossRef]
32. Song, J.; Lee, J.H.; Kim, D.; Kim, Y.; Jung, S. Analysis and Modeling of Concentrated Winding Variable Flux Memory Motor Using Magnetic Equivalent Circuit Method. *IEEE Trans. Magn.* **2017**, *53*, 1–4. [CrossRef]
33. Ura, A.; Sanada, M.; Morimoto, S.; Inoue, Y. Influence of Structural Differences on Motor Characteristics of Concentrated Winding IPMSMs Obtained by Automatic Design. *IEEJ J. Ind. Appl.* **2019**, *8*, 458–464. [CrossRef]
34. Wang, J.; Howe, D. Tubular modular permanent-magnet machines equipped with quasi-halbach magnetized magnets-part i: Magnetic field distribution, emf, and thrust force. *IEEE Trans. Magn.* **2005**, *41*, 2470–2478. [CrossRef]
35. Sim, M.-S.; Ro, J.-S. Semi-Analytical Modeling and Analysis of Halbach Array. *Energies* **2020**, *13*, 1252. [CrossRef]
36. Duong, M.-T.; Chun, Y.-D.; Bang, D.-J. Improvement of Tubular Permanent Magnet Machine Performance Using Dual-Segment Halbach Array. *Energies* **2018**, *11*, 3132. [CrossRef]

Publisher's Note: MDPI stays neutral with regard to jurisdictional claims in published maps and institutional affiliations.

© 2020 by the authors. Licensee MDPI, Basel, Switzerland. This article is an open access article distributed under the terms and conditions of the Creative Commons Attribution (CC BY) license (http://creativecommons.org/licenses/by/4.0/).